Atmospheric Research 225 (2019) 181–192

Contents lists available at ScienceDirect

Atmospheric Research

journal homepage: www.elsevier.com/locate/atmosres

# Global validation of columnar water vapor derived from EOS MODIS-MAIAC algorithm against the ground-based AERONET observations

Vitor S. Martins[a,*], Alexei Lyapustin[b], Yujie Wang[b,c], David M. Giles[d,b], Alexander Smirnov[d,b], Ilya Slutsker[d,b], Sergey Korkin[e]

[a] Agricultural and Biosystems Engineering, Iowa State University, Ames, IA, USA
[b] NASA Goddard Space Flight Center, Greenbelt, MD, USA
[c] Joint Center for Earth systems Technology (JCET), University of Maryland-Baltimore County (UMBC), Baltimore, MD, USA
[d] Science Systems and Applications, Inc., Lanham, MD, USA
[e] Universities Space Research Association (USRA) GESTAR, Columbia, MD, USA

ARTICLE INFO

*Keywords:*
MCD19A2
MODIS Collection 6
MAIAC water vapor
Time series analysis

ABSTRACT

The water vapor is a relevant greenhouse gas in the Earth's climate system, and satellite products become one of the most effective way to characterize and monitor the columnar water vapor (CWV) content at global scale. Recently, a new product (MCD19) was released as part of MODIS (Moderate Resolution Imaging Spectroradiometer) Collection 6 (C6). This operational product from Multi-Angle Implementation for Atmospheric Correction (MAIAC) algorithm includes a high 1 km resolution CWV retrievals. This study presents the first global validation of MAIAC C6 CWV obtained from MODIS MCD19A2 product. This evaluation was performed using Aerosol Robotic Network (AERONET) observations at 265 sites (2000–2017). Overall, the results show a good agreement between MAIAC/AERONET CWV retrievals, with correlation coefficient higher than 0.95 and RMS error lower than 0.250 cm. The binned error analysis revealed an underestimation (~10%) of Aqua CWV retrievals with negative bias for CWV higher than 3.0 cm. In contrast, Terra CWV retrievals show a slope of regression close to unity and a low mean bias of 0.075 cm. While the accuracy is relatively similar between 1.0 and 5.0 cm for both sensor products, Terra dataset is more reliable for applications in humid tropical areas (> 5.0 cm). The expected error was defined as ± 15%, with > 68% of retrievals falling within this envelope. However, the accuracy is regionally dependent, and lower error should be expected in some regions, such as South America and Oceania. Since MODIS instruments have exceeded their design lifetime, time series analysis was also presented for both sensor products. The temporal analysis revealed a systematic offset of global average between Terra and Aqua CWV records. We also found an upward trend (~0.2 cm/decade) in Terra CWV retrievals, while Aqua CWV retrievals remain stable over time. The sensor degradation influences the ability to detect climate signals, and this study indicates the need for revisiting calibration of the MODIS bands 17–19, mainly for Terra instrument, to assure the quality of the MODIS water vapor product. Finally, this study presents a comprehensive validation analysis of MAIAC CWV over land, raising the understanding of its overall quality.

## 1. Introduction

Water vapor is the most abundant greenhouse gas in the Earth-atmosphere system and plays a significant role in the Earth's climate (Held and Soden, 2000; IPCC, 2007; Dessler and Wong, 2009). This constituent drives a strong positive feedback in the climate system (Colman, 2003; Dessler et al., 2008). According to IPCC (2007), the tropospheric water vapor is increasing as a response to higher temperature (↑anthropogenic emissions) over both land and ocean. The increased water vapor can considerably amplify climate warming effects caused by the greenhouse emissions, such as $CO_2$, $CH_4$ and others (Rind et al., 1991; Soden, 2000; Dessler and Wong, 2009). In addition, atmospheric water vapor content is a key factor defining the local humidity, cloud formation, and hydrological cycle, especially in the precipitation regimes (Allan and Soden, 2008). The water vapor content strongly varies in both space and time. For instance, the atmosphere of the warm and humid tropical regions holds a large amount of water vapor (up to 6 cm), which decreases rapidly in mid- and high-latitudes. The large variety of sources (e.g. ocean evaporation and plant transpiration) and complex dynamic of moisture transport present a

* Corresponding author.
*E-mail addresses:* vitors@iastate.edu (V.S. Martins), alexei.i.lyapustin@nasa.gov (A. Lyapustin).

https://doi.org/10.1016/j.atmosres.2019.04.005
Received 4 December 2018; Received in revised form 6 April 2019; Accepted 7 April 2019
Available online 08 April 2019
0169-8095/ 

challenge for modeling the columnar water vapor (CWV) across the world (Trenberth et al., 2005; Sherwood et al., 2010). Therefore, extensive monitoring of this constituent is highly required to the understanding of the climate change in coming years.

Several ground-based stations have been established to monitor the seasonal variability of CWV using conventional methods, such as radiosondes (Durre et al., 2006; Seidel and Randel, 2006), Global Positioning System (GPS) receivers (Bevis et al., 1992; Rocken et al., 1993), and sunphotometer networks (Halthore et al., 1997; Alexandrov et al., 2009). These techniques provide the most accurate estimation of water vapor, supporting many studies focused on climate and hydrology analysis (Torres et al., 2010; Ortiz de Galisteo et al., 2014; Gui et al., 2017; Fragkos et al., 2018). However, these traditional measurements are local and sparse, and the spatial coverage is often limited for remote areas, such as Amazon rainforest, Sahara Desert and poles. In this context, satellite data offer the most powerful way to provide daily global observations of land and atmosphere dynamic. Over the last two decades, a number of satellites sensors have been used to estimate the CWV content, including near-infrared (NIR) sensors (e.g. Moderate Resolution Imaging Spectroradiometer (MODIS)), and microwave sensors (e.g. Advanced Microwave Scanning Radiometer). These instruments and others meteorological sensors are a unique data source for large-scale CWV studies.

MODIS instrument is a 36-channel imaging radiometer on board NASA's Terra and Aqua satellites, launched in December 1999 and May 2002, respectively. MODIS offers a large inter-disciplinary suite of scientific products developed for land, ocean and atmospheric studies (e.g. King et al., 1992). Particularly, standard MODIS Level-2 water vapor product, namely the MOD05 (Terra) and MYD05 (Aqua), delivers near-daily global CWV retrievals based on the differential absorption technique (Frouin et al., 1990; Kaufman and Gao, 1992; Gao and Kaufman, 2003). This technique quantifies the degree of water vapor absorption in the MODIS NIR channels using the ratio of measured radiance from absorbing channels (0.905, 0.936, and 0.940 μm) against nearby channels in “atmospheric windows” (0.865 and 1.240 μm) (Schläpfer et al., 1998). The column water vapor is estimated from the total two-way water vapor transmittance using the look-up-table (LUT) (Schmid et al., 1996). Gao and Kaufman (2003) found that the expected error of MOD05 water vapor is about 5–15%. The authors mentioned that main uncertainties are related to (i) surface reflectance properties, (ii) calibration issues, (iii) atmospheric profiles (temperature and moisture), and (iv) cloud contamination. Several studies have evaluated the MOD05 product at regional-scale (Prasad and Singh, 2009; Gui et al., 2017; Vaquero-Martínez et al., 2017, 2018; Shi et al., 2018). Recently, Bright et al. (2018) performed a global-scale validation of MODIS CWV product using AERONET observations, and they found a correlation of R ~ 0.83 and RMSE of ~0.521 (Terra) and 0.607 cm (Aqua). The authors also mentioned the overestimation at larger magnitudes (> 3 cm).

A new set of MODIS surface-atmosphere products from the Multi-Angle Implementation for Atmospheric Correction (MAIAC) algorithm was released in late May 2018 (Lyapustin et al., 2011, 2012, 2018). This algorithm delivers a suite of gridded atmosphere-surface products at 1 km resolution over global land. The MAIAC MODIS Collection 6 products are reported in two land files (MCD19A1 for surface reflectance, and MCD19A3 for BRDF/albedo) and atmospheric properties file (MCD19A2) (Lyapustin et al., 2018). Among others, MCD19A2 includes a column water vapor based on MODIS NIR bands at 0.94 μm region (Lyapustin et al., 2014a, 2014b). This algorithm is a modified version of Gao and Kaufman (2003). While MOD05 algorithm applies two additional MODIS channels (0.865 and 1.24 μm) to estimate surface reflectance in absorbing channels, MAIAC follows a more straightforward method using only 3 NIR bands to avoid the assumption of the spectral linearity of the surface reflectance in the 0.87 and 1.24 μm interval. According to Lyapustin et al. (2014a), this approach is more stable and achieves similar or better performance compared to the MOD05 product. In addition, MAIAC cloud mask algorithm provides an accurate cloud detection (Lyapustin et al., 2008), which reduces the noise in the clear-pixel CWV retrievals, especially over tropics (Hilker et al., 2012).

Previous validation of MAIAC CWV retrievals revealed a good agreement with the Aerosol Robotic Network (AERONET) measurements across South America (R ~ 0.97, RMSE ~0.345 cm) (Martins et al., 2017a). Since this operational data product is now available as part of the MODIS Collection 6 (C6), a more complete evaluation is required to support user's applications. This study presents a global validation of columnar water vapor retrievals from MODIS C6 MAIAC (MCD19A2) product. A total of 265 AERONET sites were used to evaluate the cloud-free CWV retrievals over land. The MCD19A2 products were obtained for nearly the entire MODIS mission (2000–2017). The validation was performed at multiple spatial scales (global, regional and local), and includes the time series analysis. Note that previous validation of MAIAC CWV (Terra) retrievals was performed for the single-year dataset (2003) using 156 AERONET sites (Lyapustin et al., 2008), but this paper is the first global analysis of MCD19A2 CWV exploring this product for the near-entire mission. This paper is structured as follows: Section 2 presents the satellite product (MCD19A2) and ground-truth dataset (AERONET), including the description of match-up procedure. The results are presented in Section 3, with global, regional and local validation analysis. Further, temporal evaluation is also presented in this section, followed by a discussion in Section 4. The summary and conclusions are drawn in the last section.

## 2. Data and methods

### 2.1. MODIS-MAIAC water vapor (MCD19A2)

MODIS instruments were launched on board of NASA Earth Observing System (EOS) Terra and Aqua satellites. The Terra and Aqua operate on sun-synchronous orbit (~705 km altitude), with local equator crossing at approximately 10:30 am (descending node) and 01:30 pm (ascending node), respectively. The MODIS instrument provides near-daily global observations in 36 channels (0.415–14.23 μm), wide swath (2230 km), and three spatial resolutions at nadir (250, 500 and 1000 m). This sensor offers a unique design to support the generation of multidisciplinary products (Justice et al., 1998; Parkinson, 2013). As part of MODIS Level-2 products, MCD19A2 is a combined MODIS C6 Terra and Aqua product derived from MAIAC algorithm (Lyapustin et al., 2018). This new product contains multiple scientific data sets (SDS), such as aerosol optical depth at 0.470 and 0.550 μm, columnar water vapor, and cloud mask at 1 km resolution. As mentioned earlier, MAIAC CWV algorithm is based on the heritage of MOD05 product (Gao and Kaufman, 2003). This approach uses two 2-channel ratios in the 0.940 um region to compute the total water vapor transmittance, and then, the inversion of CWV is performed based on LUT procedures. The spectral channels used in this algorithm are MODIS B17 (0.890–0.920 μm), B18 (0.931–0.941 μm), and B19 (0.915–0.965 μm). Since the sensitivity to water vapor absorption varies between these channels, weighting function is also implemented to explore this variability in dry or humid condition. A detailed description of MAIAC CWV algorithm can be found in Lyapustin et al. (2014a,b, 2018).

In this study, MCD19A2 data were obtained from the Level-1 and Atmosphere Archive & Distribution System (LAADS) Distributed Active Archive Center (DAAC) (data portal: https://ladsweb.modaps.eosdis.nasa.gov/). The daily MCD19A2 products were acquired for nearly the entire mission (2000–2017) across the world (total raw data ~ 10.7 Tb). These data products are delivered as standard MODIS tiles in HDF4 files (see Lyapustin et al., 2018). The SDSs are stored as multidimensional arrays with the third dimension representing the number of orbit overpasses (“Orbit_amount”). We extracted MAIAC Terra ($MAIAC_T$) and MAIAC Aqua ($MAIAC_A$) CWV from MCD19A2 product. Note that

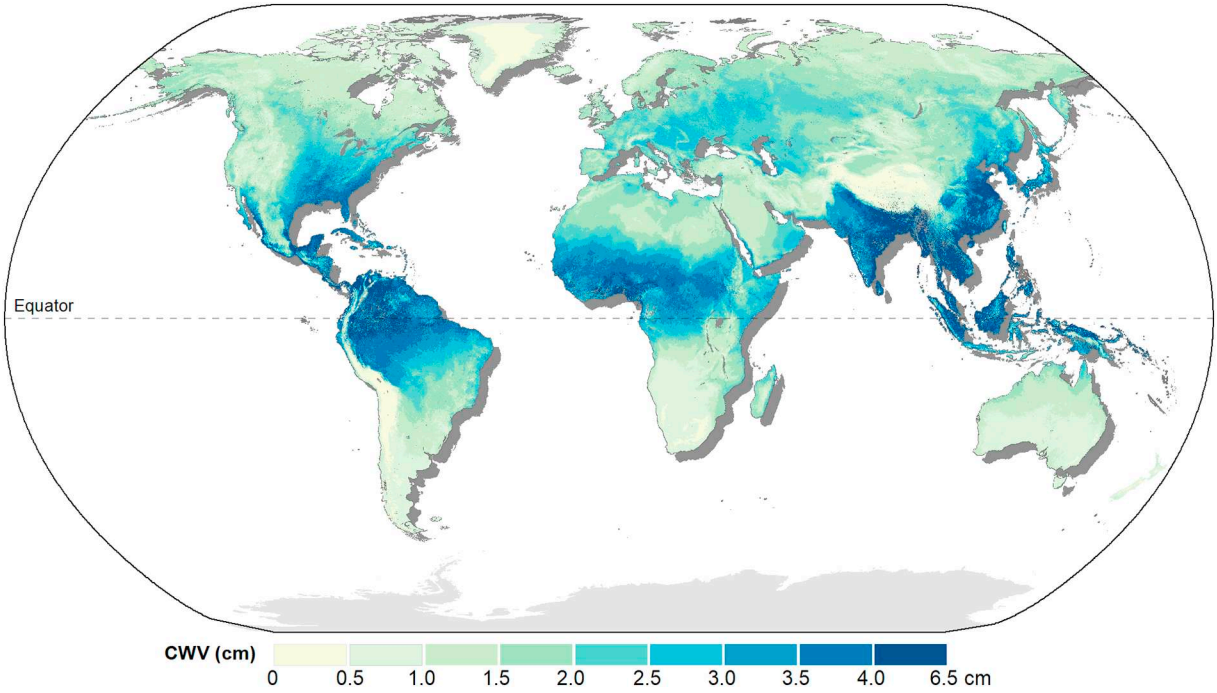


**Fig. 1.** Global average of columnar water vapor (CWV) derived from MAIAC Terra (MCD19A2) from July 2004.

MCD19A2 product is referred as MAIAC hereafter. The global attributes provide the orbit information ("Orbit_time_stamp") to separate Terra and Aqua products from a multidimensional array. The quality assurance (QA) was also extracted from SDS "AOD_QA" layer for each orbit. The high-quality retrievals were selected by excluding cloud and adjacent to cloud pixels. Therefore, the basic processing is described as follow: (i) extraction of $MAIAC_T$ and $MAIAC_A$ CWV retrievals from MCD19A2 file; (ii) conversion by scaling factor (0.001); (iii) filtering the cloud-free retrievals using QA flags. In addition, we computed the monthly global average from daily $MAIAC_T$ and $MAIAC_A$ CWV observations, and then, these averages were used to long-term evaluation of both products (Section 3.3). Fig. 1 illustrates the global CWV derived from $MAIAC_T$ in July 2004.

### 2.2. AERONET data

The AErosol RObotic NETwork (AERONET) is a worldwide network (http://aeronet.gsfc.nasa.gov) of sun-photometers that provides routine measurements of direct sun and sky radiance for retrieval of aerosol (primarily) and water vapor properties (Holben et al., 1998; Dubovik et al., 2002). The AERONET network includes well-established monitoring sites (> 400) in a wide variety of atmospheric conditions across the world. The Cimel sun-photometers measure the sun/sky radiance at every 15 min in multiple spectral channels (0.340, 0.380, 0.440, 0.500, 0.675, 0.870, 1.020, and 1.640 μm), including the water vapor absorbing band (0.940 μm). The AERONET version 3.0 is distributed with three quality levels (Giles et al., 2019): Level 1.0 (raw data), Level 1.5 (cloud-screened and quality controlled), and Level 2.0 (cloud-screened and quality-assured). Because the long-term dataset (> 25 years) and standard quality protocols, numerous studies have applied this dataset as ground-truth reference for validating MODIS water vapor products (Bennouna et al., 2013; Diedrich et al., 2015; Shi et al., 2018; Bright et al., 2018).

Although the AERONET is primarily focused on the aerosol optical properties, CWV retrievals are also derived from these network measurements (Holben et al., 1998; Giles et al., 2019). The AERONET water vapor algorithm uses the Beer-Lambert-Bouguer attenuation Law and modeled water vapor transmittance in absorption band (0.940 μm) to retrieve the CWV values (Michalsky et al., 2001; Reagan et al., 1995; Schmid et al., 1996; Halthore et al., 1997). Eq. 1 represents the output instrument voltage V(λ) in the absorption band (λ = 0.940 μm) as (Schmid et al., 2001):

$$V(\lambda) = V_o(\lambda).\, d^{-2}.\, \exp[-m.\, \tau(\lambda)].\, T_w(\lambda) \quad (1)$$

$$T_w(\lambda) = \exp[-a.\, (m_w.\, W)^b] \quad (2)$$

where $V_o$ is calibration constant of the instrument, d is relative Earth-Sun distance in astronomical units (AU), m is relative air mass (without water vapor), $\tau$ is the total optical depth (gases and aerosol), and $m_w$ is the air mass of water vapor. The water vapor (W) is retrieved from modeled water vapor transmittance (Tw) using three parameters expression (Eq. 2). The two coefficients "a" and "b" are modeled by the IPC method (Lyapustin, 2003) according to instrument design, such as filter response functions. The correction of aerosol effects at 0.940 μm channel is performed by Ångström extrapolation from 0.440–0.870 μm interval.

The AERONET CWV data (level 2.0, version 3.0) were acquired from 265 sites across all continents (Fig. 2). The selected sites have at least three years of quality-assured retrievals within 2000–2017 period. These AERONET records were used as ground-truth reference to validate MAIAC CWV retrievals. To clarify, CWV value represents the total water vapor mass per unit area in the vertical column of atmosphere (unit: cm or $g.cm^{-2}$). Note that AERONET retrievals are relatively similar to other traditional measurements. For example, Pérez-Ramírez et al. (2014) found a small bias (~0.06–0.10 cm) between AERONET and GPS retrievals for three sites. Similarly, Bokoye et al. (2007) estimated the mean bias of $-0.09 \pm 0.16$ cm between these methods in Canada. The total uncertainty of sun-photometer retrievals was estimated as < 10% (Smirnov et al., 2004; Pérez-Ramírez et al., 2014; Alexandrov et al., 2009), but it may offer some improvement in this uncertainty due to algorithm refinements in version 3.0 CWV (Giles et al., 2019).

### 2.3. Collocation procedure and validation analysis

The collocation procedure describes the match-up criteria between satellite and sun-photometer measurements within spatial and temporal

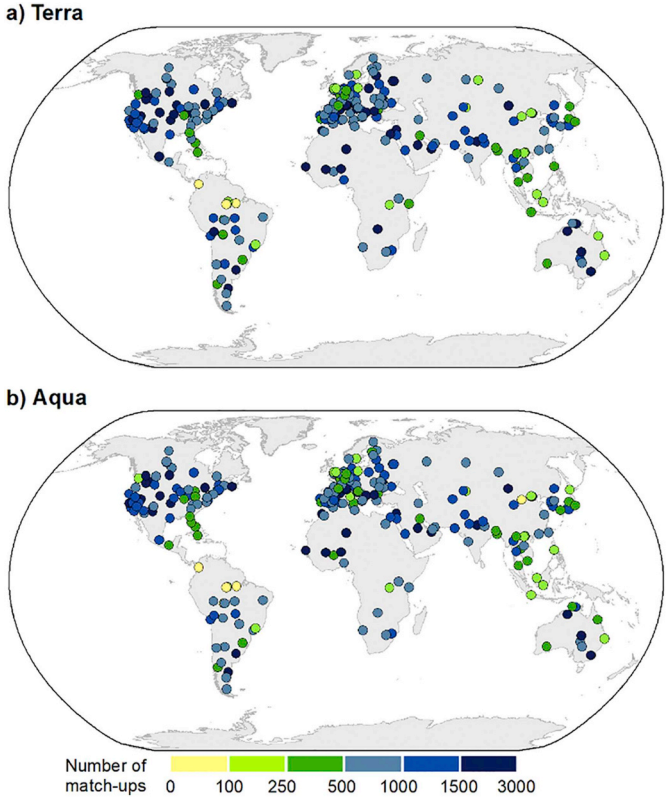


**Fig. 2.** Number of match-ups between MAIAC and AERONET CWV measurements for each site.

window (Chu et al., 2002). This procedure was adapted from Lyapustin and Wang (2008). The spatial average of MAIAC CWV was computed using 9 × 9 pixels (~1 × 1 km per pixel) around each selected site. This satellite average was then compared to the temporal average of AERONET CWV measurements within ± 30 min of the satellite overpass. Fig. 1 shows the number of match-ups between MAIAC and AERONET records for each site. The number of match-ups is mostly dependent on the AERONET data availability and cloud-free satellite retrievals for each region. Note that selected sites represent a diversity of conditions (land and atmospheric) across the world, giving a robust dataset for this validation.

The validation analysis uses the common statistical metrics, such as Root Mean Square Error (RMSE), relative error (R), mean bias as presented in the Eqs. 4, 5 and 6, respectively. The binned-CWV analysis (1.0 cm intervals) is also presented for evaluating dry and wet biases. In addition, the expected error (EE) of MAIAC CWV was defined as ± 15%, where the error envelope is expected to contain > 68% of retrievals (one standard deviation σ) assuming an approximation to the Gaussian error distribution. This assumption supports the definition of this minimum threshold (68%), but the number of retrievals falling within EE envelope is expected to be higher due to peak of error values near zero. The EE envelope is typically used in aerosol context, and further applications of this metric are presented in Remer et al. (2005) and Levy et al. (2010). This symmetrical envelope includes the uncertainties related to land surface properties, aerosol effects, modeled absorption coefficients, and calibration errors.

$$RMSE = \sqrt{\frac{1}{N}\sum_{i=1}^{N}(CWV_{MAIAC} - CWV_{AERONET})^2} \quad (3)$$

$$RE = \frac{1}{N}\sum_{i=1}^{N}\frac{|CWV_{MAIAC} - CWV_{AERONET}|}{CWV_{AERONET}} \times 100 \quad (4)$$

$$\text{Mean bias} = \frac{1}{N}\sum_{i=1}^{N}(CWV_{MAIAC} - CWV_{AERONET}) \quad (5)$$

where $CWV_{MAIAC}$ and $CWV_{AERONET}$ represent MAIAC and AERONET retrievals, respectively; and $N$ is the number of match-ups.

## 3. Results

### 3.1. Global performance of MAIAC water vapor (MCD19A2)

Fig. 3 shows the scatter plots of MAIAC CWV Terra (a) and Aqua (b) against ground-based AERONET observations. The summary statistics of this comparison is given in Table 1. The binned-CWV analysis is also presented to explore the signal-dependent error. This global validation includes 290,389 and 259,856 match-ups for $MAIAC_T$ and $MAIAC_A$ across all continents, respectively. The collocated data range from 0 to 6 cm, with most of its samples within 0–2 cm interval. Note that 265 AERONET sites were used in this global analysis, covering distinct water vapor conditions such as Amazon rainforest and Sahara Desert. As mentioned earlier, the subscript "T" and "A" represent Terra and

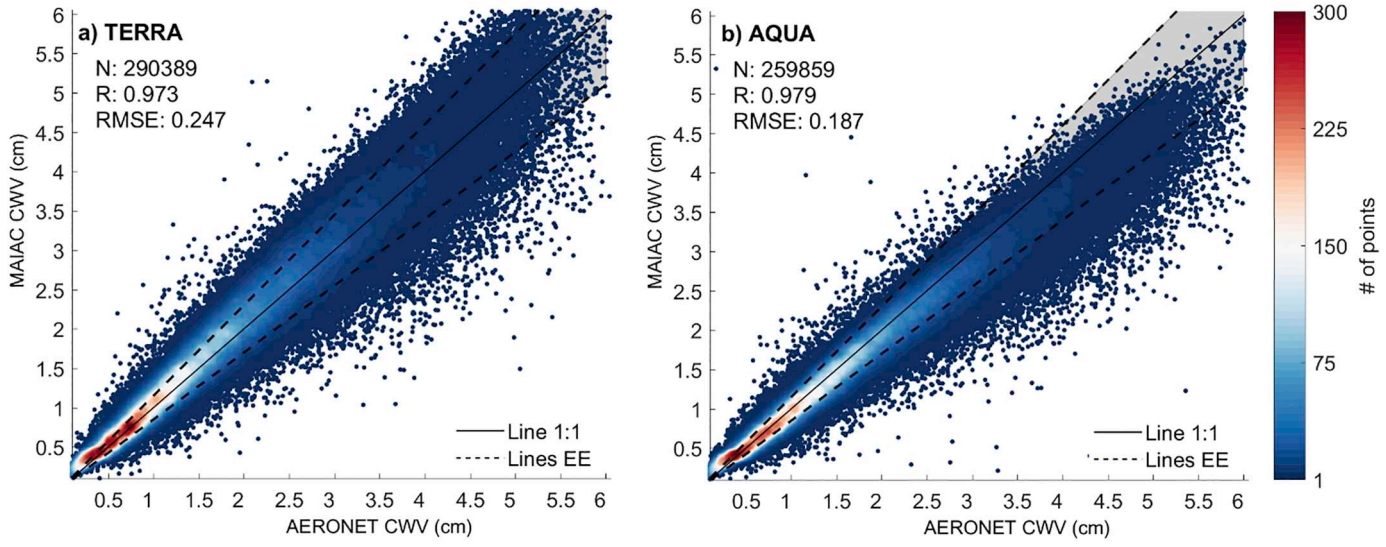


**Fig. 3.** Scatter plots of CWV (cm) derived from MAIAC (MCD19A2) product versus simultaneous AERONET observations for all sites. The solid line represents the line 1–1, dashed lines are the envelope of expected error. The summary statistics are presented in Table 1.

**Table 1**
Summary statistics of global validation of MAIAC CWV retrievals. These metrics were calculated using all match-ups. The $\beta_1$ and $\beta_0$ are the slope and intercept of linear regression, respectively; and EE is the fraction of retrievals within error of ± 15%.

| Intervals | N | $\beta_1$ | $\beta_0$ | R | Mean bias (cm) | RMSE (cm) | RE (%) | EE (%) | | |
|---|---|---|---|---|---|---|---|---|---|---|
| | | | | | | | | within | above | below |
| TERRA | | | | | | | | | | |
| 0–1.0 | 98,617 | 0.954 | 0.085 | 0.921 | 0.057 | 0.96 | 18.3 | 58.7 | 38.0 | 3.4 |
| 1.0–2.0 | 107,222 | 1.071 | −0.009 | 0.856 | 0.094 | 0.184 | 11.0 | 72.9 | 23.4 | 3.7 |
| 2.0–3.0 | 53,473 | 0.952 | 0.228 | 0.672 | 0.112 | 0.295 | 10.3 | 75.4 | 19.4 | 5.2 |
| 3.0–4.0 | 20,588 | 0.909 | 0.346 | 0.509 | 0.036 | 0.437 | 10.1 | 76.4 | 13.4 | 10.3 |
| 4.0–5.0 | 8682 | 1.004 | −0.049 | 0.420 | −0.032 | 0.595 | 10.6 | 74.4 | 11.4 | 14.2 |
| > 5.0 cm | 1807 | 0.671 | 1.589 | 0.264 | −0.173 | 0.743 | 11.2 | 73.1 | 8.5 | 18.4 |
| **All (0–6.0)** | 290,389 | 0.991 | 0.089 | 0.973 | 0.075 | 0.247 | 13.3 | 68.8 | 26.4 | 4.7 |
| AQUA | | | | | | | | | | |
| 0–1.0 | 89,419 | 0.858 | 0.098 | 0.927 | 0.012 | 0.083 | 14.8 | 69.6 | 23.7 | 6.7 |
| 1.0–2.0 | 96,458 | 0.948 | 0.031 | 0.882 | −0.044 | 0.144 | 7.8 | 87.5 | 3.0 | 9.5 |
| 2.0–3.0 | 47,385 | 0.837 | 0.255 | 0.736 | −0.141 | 0.217 | 8.1 | 85.8 | 0.8 | 13.5 |
| 3.0–4.0 | 17,480 | 0.759 | 0.491 | 0.545 | −0.331 | 0.329 | 10.7 | 74.6 | 0.3 | 25.1 |
| 4.0–5.0 | 7544 | 0.766 | 0.467 | 0.445 | −0.565 | 0.427 | 13.1 | 63.4 | 0 | 36.6 |
| > 5.0 cm | 1573 | 0.639 | 1.050 | 0.363 | −0.884 | 0.511 | 16.5 | 46.7 | 0 | 53.3 |
| **All (0–6.0)** | 259,859 | 0.871 | 0.123 | 0.979 | −0.082 | 0.187 | 10.7 | 79.2 | 9.4 | 11.4 |

Aqua products, respectively. In general, we found a good correlation of MAIAC and AERONET measurements, with $R_T$ of 0.973 and $R_A$ of 0.979. The slope of linear fit indicates a slight underestimation of $MAIAC_A$ retrievals (0.871), while $MAIAC_T$ presents slope close to unity (0.991). The RMSE is lower than 0.250 cm for both Terra and Aqua retrievals, especially for $MAIAC_A$ (0.187 cm). These findings are a positive measure for this satellite-derived product. However, it should be interpreted with caution because the errors depend on the water vapor amount (see more in Section 3.3). The binned-CWV analysis shows that statistical errors vary from low- to high-CWV bins (Table 1). For instance, $MAIAC_A$ has a good agreement with the AERONET data for dry condition (up to 1.0 cm), but some underestimation is observed in wet condition (> 5.0 cm). In contrast, we found that $MAIAC_T$ performance is better for high-CWV values ($EE_T$ ~ 73%) compared to $MAIAC_A$ ($EE_A$ ~46.7%) (Table 1). Therefore, the overall comparison shows a good performance of MAIAC CWV retrievals, but the statistical errors vary according to the water vapor abundance and sensor.

The results confirm that both products provide > 68% (one standard deviation) of retrievals falling within EE confidence envelope ( ± 15%). The high-quality CWV retrievals are typically observed from 1.0 to 5.0 cm; EE values range from 69.6 to 87.5% for both sensor products. This is a relevant result for water vapor product given the natural dominance of this range (1.0–5.0 cm). The overall analysis suggests a better performance of $MAIAC_A$ (within EE = 79.2%) compared to $MAIAC_T$ (within EE = 68.8%), but it should be noted that $MAIAC_A$ retrievals underestimate the high-CWV values. To clarify, further analysis of mean bias (MAIAC – AERONET) is given in Fig. 5. The solid line represents the EE envelope of ± 15% and red dots are the mean bias. Overall, we observed that the mean differences of $MAIAC_T$ and AERONET observations are close to zero. In contrast, a dry bias (underestimation) was found in $MAIAC_A$ retrievals with bias increasing with atmospheric CWV. Consequently, the percentage of $MAIAC_A$ retrievals falling in the EE envelope is lower than 50% for CWV ≥ 5.0 cm. These findings are relevant for studies focusing on tropical regions (high humidity) because it suggests that $MAIAC_T$ dataset is more suitable at high-CWV compared to $MAIAC_A$. In addition, Fig. 4 presents the histogram distribution of mean bias using all collocated data for both sensor products. Overall, our results show a lower mean absolute bias of

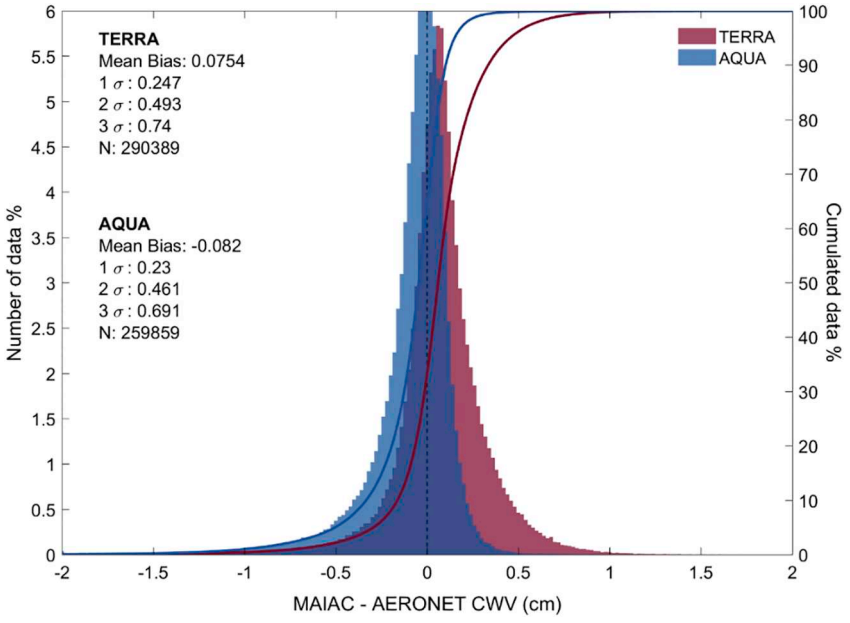


**Fig. 4.** Histogram of mean bias (or difference) between MAIAC (MCD19A2) and AERONET CWV retrievals using all collocated data.

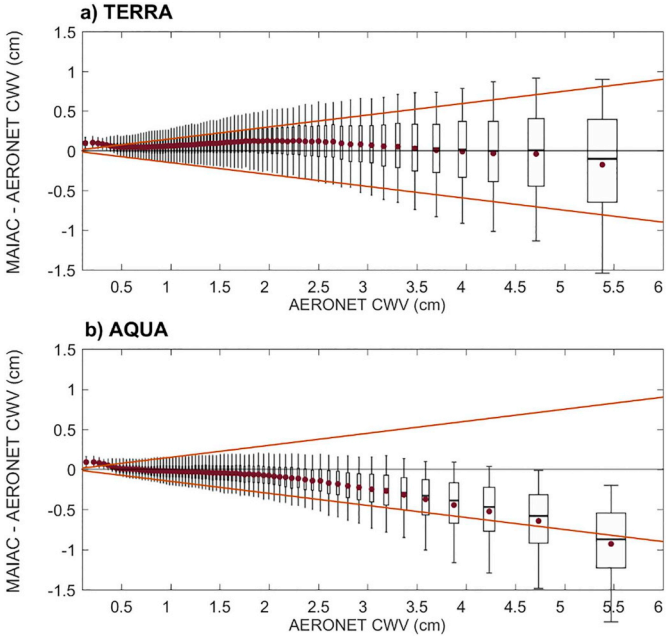


**Fig. 5.** Mean bias between MAIAC (MCD19A2) and AERONET CWV retrievals: Terra (a) and Aqua (b). The expected error envelope ( ± 15%) is shown in solid lines. Each box edge and whiskers represent the 25–75% and 5–95% of data with median (black line) and mean (red point). (For interpretation of the references to colour in this figure legend, the reader is referred to the web version of this article.)

$MAIAC_T$ (0.075 cm) compared to $MAIAC_A$ retrievals (0.082 cm). Both $MAIAC_T$ and $MAIAC_A$ bias distributions are centered near zero. However, $MAIAC_T$ shows a small positive bias, while $MAIAC_A$ bias distribution is left-skewed towards more negative values. The histograms approximate a normal distribution (e.g.: symmetrical bell-shaped curve), but according to the goodness of fit for normality (Kolmogorov-Smirnov test), it does not follow a normal (gaussian) distribution at the 5% significance level. The overall MAIAC CWV bias is low (< 0.1 cm), with one standard deviation < 0.25 cm.

### 3.2. Local and regional performance

Fig. 6 shows geographical distribution of MAIAC/AERONET comparison statistics. In general, a strong correlation (R > 0.95) was found in 231 ($MAIAC_A$) and 221 sites ($MAIAC_T$) across the world. These positive results were mainly observed in the sub-tropical region (see dark blue dots in Fig. 6a). For few sites, the correlation coefficient was lower than 0.75 (Belterra (2.65°S, 54.95°W) and Kuching (1.49°N, 110.35°E)). These AERONET stations are located in the cloudy tropical region, where the errors of MAIAC cloud detection become noticeable. Further, we observed low mean biases (up to ± 0.1) over 126 sites ($MAIAC_T$) and 170 sites ($MAIAC_A$). By considering the wide variability of CWV values (0 to 6 cm), the typical error is quite reasonable for most applications across the world.

In the local analysis, we also demonstrate that Aqua CWV retrievals are generally "drier" compared to AERONET observations; negative mean biases were observed for 208 out of 265 sites. In contrast, $MAIAC_T$ CWV retrievals show a positive mean bias over most of AERONET locations (214 out of 265 sites). These results suggest that users should expect an underestimation of CWV from Aqua over sub-tropical (up to −0.25 cm) and tropical (up to −0.75 cm) areas, while Terra retrievals tend to overestimate the CWV values. In addition, the RMSE is typically < 0.25 cm over 206 (Terra) and 228 (Aqua) sites. The particular low RMSE values were observed across North America, Europe, and Central Asia. The range of RMSE values (Fig. 6c) varies significantly from sub-tropical (up to 0.3 cm) to tropical sites (up to 0.6 cm). These regional differences are quite expected because the large variability of water vapor magnitude among regions. Moreover, it should note that similar RMSE values are often observed for Terra and Aqua products at the site level despite different mean bias. For example, MAIAC/AERONET comparison shows an RMSE of 0.093 (Terra) and 0.096 (Aqua) at Valladolid site (41.66°N, 4.71°W).

The EE for each site is mapped in Fig. 6d. Notably, the number of sites exceeding the EE of 68% is higher for $MAIAC_A$ retrievals (213 sites) compared to $MAIAC_T$ (145 sites). This is visually illustrated by the blue dots (Fig. 6d). As mentioned earlier, MAIAC accuracy varies between regions (e.g. sub-tropical versus tropical sites), but statistical metrics should be interpreted with caution, especially in the tropical region. For example, despite the poor correlation and high RMSE of MAIAC/AERONET comparison in tropical region (23°N – 23°S), some sites present a remarkable EE values, such as Balbina ($EE_T$ = 73.3%), Bac-Lieu ($EE_T$ = 74.8%), and CRPSM-Malindi ($EE_T$ = 79.6%). Similarly, we observed that ARM-Manacapuru (3.21°S, 60.59°W) in Amazon rainforest shows a relatively poor metrics (RMSE is ~0.4 cm and R is 0.774), but the EE value is satisfactory (86.6%). In contrast, there are other sites with high agreement metrics, but the retrievals do not achieve the minimum EE (see yellow dots). Therefore, we understand that it is quite difficult to make a general conclusion, but this local analysis allows the users to interpret the accuracy of specific regions and boundary conditions across continents.

Table 2 presents the summary statistics for MAIAC/AERONET comparison at the regional scale where regions are depicted in Fig. 7. The number of match-ups varies across regions, ranging from 27,133 (Africa) to 91,730 (Europe). In general, the regional performance of MAIAC retrievals is good, with a slope of linear regression close to unity and R higher than 0.92 for all regions. However, we observe that accuracy is regionally dependent (similarly to the local-scale analysis). For instance, $MAIAC_T$ showed a better agreement over Oceania, South America, North America and Europe ($EE_T$: 69.6 to 79.9%), while we observed lower $EE_T$ values (60.8 to 61.3%) over Africa, Asia, and Middle East. In contrast, $EE_A$ values are satisfactory for all regions (> 68%), with significant results in the Middle East (85.5%), Europe (82.4%) and South America (80.2%). These findings suggest that the expected error could be even lower for these regions (5–10%). Also, it should be mentioned that the regional results differ between the two sensors. For instance, the number of retrievals within EE for Terra is generally lower than EE for Aqua. Over Europe, the mean bias is 0.085 cm for Terra and −0.064 cm for Aqua. Albeit small, these differences, combined with the opposite sign of the mean bias for Terra and Aqua, could increase the uncertainty in the merged CWV product.

### 3.3. Time series analysis

This section presents the temporal assessment of the MAIAC CWV retrievals, including the seasonal and long-term monthly averages, and annual errors for both sensor products. Fig. 8 shows the latitudinal distribution of water vapor derived from $MAIAC_T$ (2000–2017) retrievals. These latitudinal averages were calculated from cloud-free CWV retrievals over land. The x-, y- and z-axis represent the months, latitudes, and CWV values, respectively. We observed an annual CWV of 3.48 ± 0.46 cm for low latitudes (10°S - 10°N) and 0.96 ± 0.43 cm ($MAIAC_T$) for high latitudes (40 - 50°). Also, the variability of water vapor is clearly different between northern and southern hemisphere throughout the year. The seasonal variability shows the northward migration of the Intertropical Convergence Zone (ITCZ) from May to October, increasing the water vapor content between 10°N and 20°N. While this analysis shows a globally-average of the water vapor distribution across the latitude, we also highlight that it varies greatly across longitude. Some areas, such as Amazon basin in South America, experience a high CWV (4.0–5.0 cm) for the most part of the year (Martins et al., 2018a), and other areas in the tropics have a drier

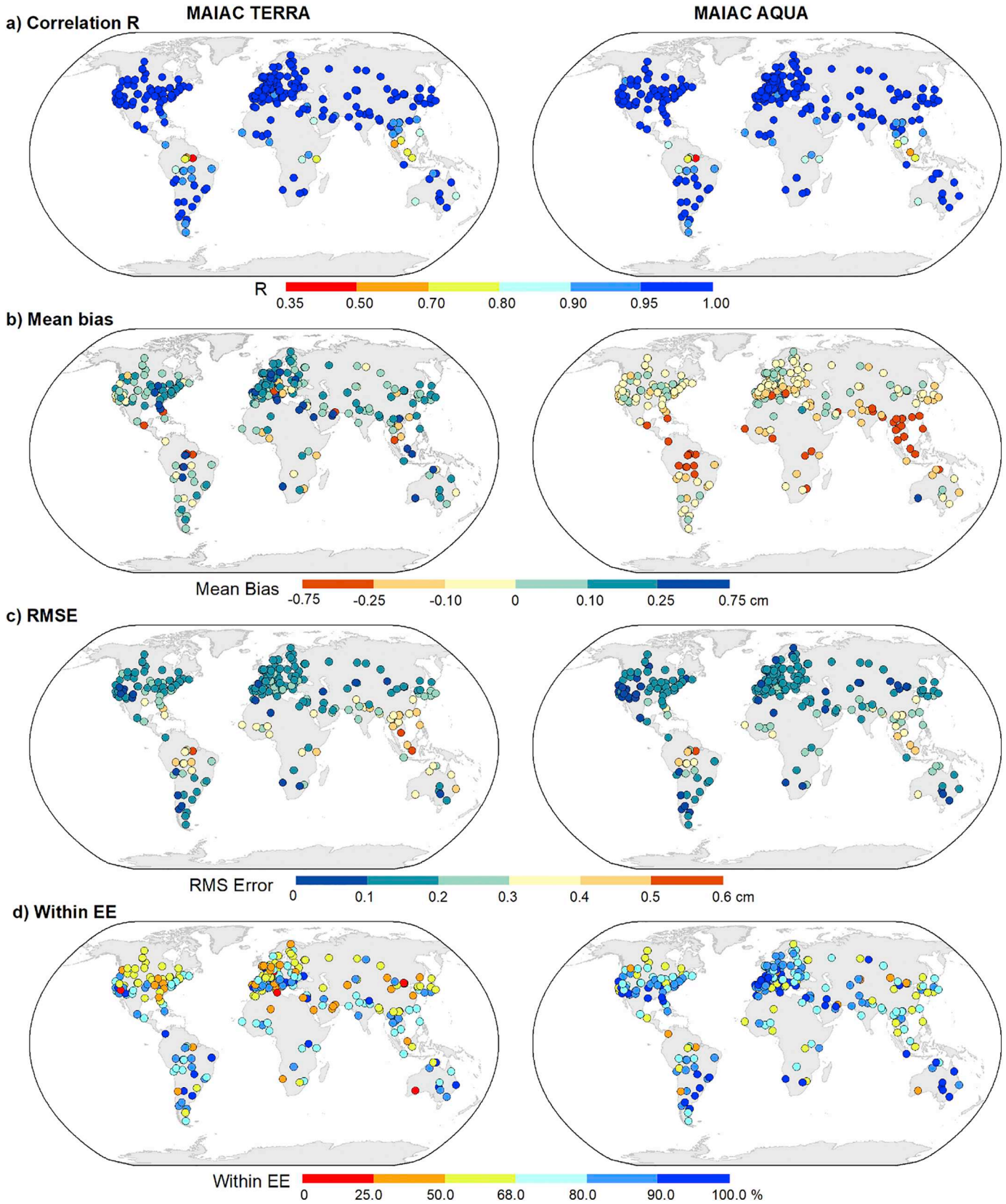


**Fig. 6.** Comparison of MAIAC/AERONET CWV retrievals for each site across the world. The statistical metrics are presented for MAIAC Terra (first column) and Aqua (second column).

**Table 2**
Regional statistics of comparison between MAIAC (MCD19A2) and AERONET CWV observations. Regions are defined in Fig. 7.

| | Number of sites | N | Slope | R | Mean bias (cm) | RMSE (cm) | RE (%) | EE (%) | | |
|---|---|---|---|---|---|---|---|---|---|---|
| | | | | | | | | within | above | below |
| TERRA | | | | | | | | | | |
| North America | 65 | 82,646 | 1.021 | 0.978 | 0.061 | 0.206 | 13.6 | 69.6 | 25.5 | 4.9 |
| South America | 27 | 20,700 | 0.993 | 0.978 | 0.037 | 0.278 | 10.3 | 79.8 | 15.0 | 5.2 |
| Europe | 79 | 91,730 | 0.997 | 0.967 | 0.085 | 0.206 | 12.4 | 69.9 | 26.0 | 4.1 |
| Africa | 23 | 27,133 | 0.931 | 0.957 | 0.087 | 0.296 | 14.4 | 60.8 | 33.1 | 6.2 |
| Asia | 35 | 33,797 | 0.994 | 0.978 | 0.082 | 0.253 | 17.1 | 61.0 | 34.7 | 4.3 |
| Middle east | 10 | 15,910 | 0.962 | 0.927 | 0.112 | 0.292 | 13.9 | 61.3 | 33.1 | 5.5 |
| Oceania | 26 | 18,473 | 0.966 | 0.963 | 0.073 | 0.365 | 10.1 | 79.9 | 15.3 | 4.9 |
| AQUA | | | | | | | | | | |
| North America | 65 | 71,463 | 0.913 | 0.985 | −0.051 | 0.150 | 11.4 | 77.6 | 12.0 | 10.4 |
| South America | 27 | 17,453 | 0.866 | 0.983 | −0.151 | 0.204 | 10.0 | 80.2 | 5.7 | 14.1 |
| Europe | 79 | 83,566 | 0.891 | 0.977 | −0.064 | 0.152 | 9.4 | 82.4 | 7.7 | 9.9 |
| Africa | 23 | 24,692 | 0.831 | 0.967 | −0.105 | 0.236 | 10.5 | 79.0 | 8.4 | 12.6 |
| Asia | 35 | 31,510 | 0.853 | 0.980 | −0.092 | 0.209 | 14.2 | 69.5 | 16.5 | 14.0 |
| Middle east | 10 | 14,328 | 0.817 | 0.956 | −0.055 | 0.192 | 8.5 | 85.5 | 5.5 | 9.1 |
| Oceania | 26 | 16,847 | 0.830 | 0.972 | −0.202 | 0.269 | 9.5 | 81.9 | 2.9 | 15.2 |

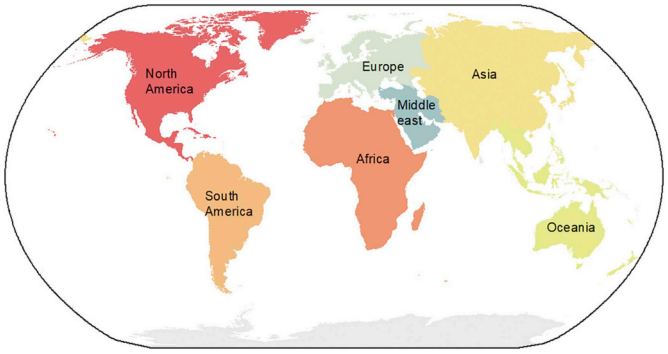


**Fig. 7.** Maps of regions used in the results of Table 2.

climate, such as Sahara Desert (< 2.0 cm). Therefore, this global evaluation provides a "big picture" of the water vapor distribution, reinforcing the potential of this new product for understanding the global climate and atmospheric dynamic.

Fig. 9 shows the global/regional time series and decadal trend of monthly CWV values derived from $MAIAC_T$ and $MAIAC_A$. The seasonal and inter-annual variability of water vapor were represented for both products at global scale, with a global water vapor ranging from 1.2 to 2.5 cm. The inter-annual variability comprises both drifting of the MODIS calibration and short-term climate events. The climate events such as La Niña (2008–2009) and El Niño (2010) have a direct impact on the interannual variability of CWV. For instance, the dry season (JJA) in Amazon presents a distinct magnitude during these climate events (see valleys in Aqua retrievals); and East US also shows lower amplitude in the seasonal pattern of CWV for La Niña years compared to El Niño. These examples illustrate the climate component influencing the interannual variability. However, the calibration drift has also a partial contribution to this temporal variability because it causes an artificial change in CWV depending on the sensor products. The results show distinct temporal trends between Terra and Aqua products: the decadal changes are higher for $MAIAC_T$ compared to $MAIAC_A$ retrievals, especially in Amazon and China (Fig. 9). We found a significant upward trend ($p < .05$) for $MAIAC_T$ over most regions (except for East North America), while no significant trend was observed for $MAIAC_A$ ($p > .05$). Also, a gradual change of offset (Terra – Aqua) was observed throughout the mission lifetime. The results illustrate that the offset values are typically lower than 0.2 cm between 2002 and 2007, and

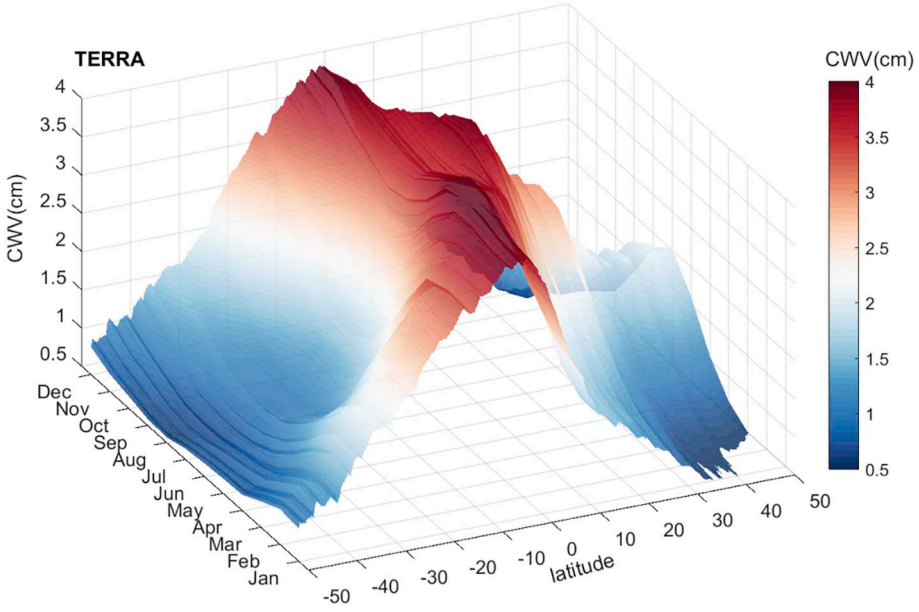


**Fig. 8.** Seasonal distribution of columnar water vapor (CWV) across latitudes. The latitudinal average was derived from global MCD19A2 Terra product over land. The x, y, z-axis represent the latitude (50°S –50°N), time (months) and averaged CWV (cm), respectively. The latitudinal gradient illustrates the variability from tropical region to high latitudes over time.

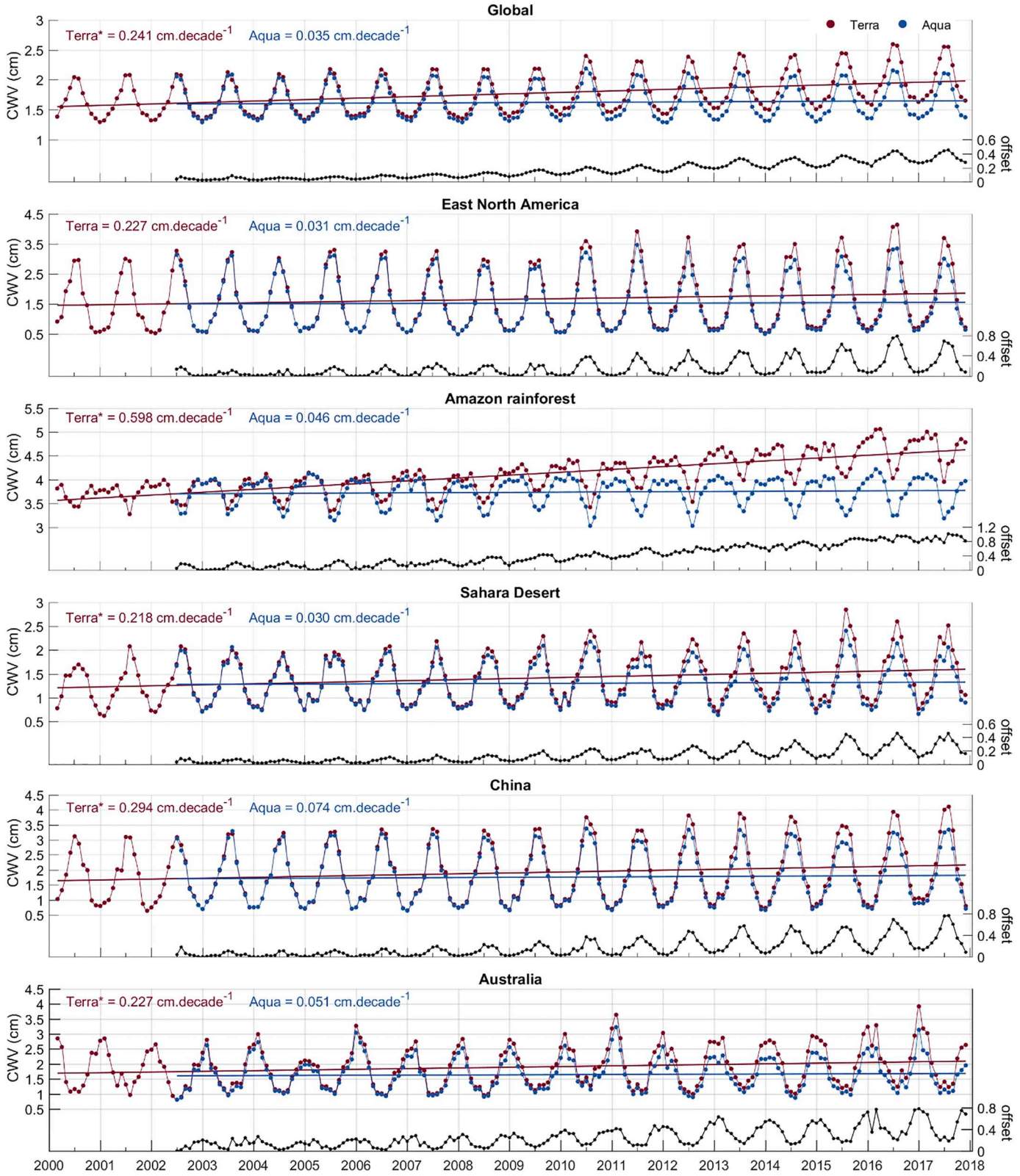


**Fig. 9.** Time series of monthly mean CWV derived from MAIAC Terra and Aqua over land. The absolute offsets (|Terra – Aqua|) CWV are presented in the bottom of each panel. The asterisk (*) indicates that calculated trend is significantly different from zero at a 95% confidence level. The bounding box of regions are described by upper left (UL) and lower right (LR) coordinates: Eastern North America (UL: 44.29°N/100.1°W; LR: 31.16°N/82.96°W), Amazon (UL: 4.24°N/72.96°W; LR: 12.65°S/48.34°W), Sahara (UL: 30.66°N/10.42°W; LR: 18.19°N/28.25°E), China (UL: 35.49°N/98.86°E; LR: 20.50°N/118.85°E), and Australia (UL: 14.84°S/121.79°E; LR: 32.35°S/145.16°E). Note that y-axis is different for each region.

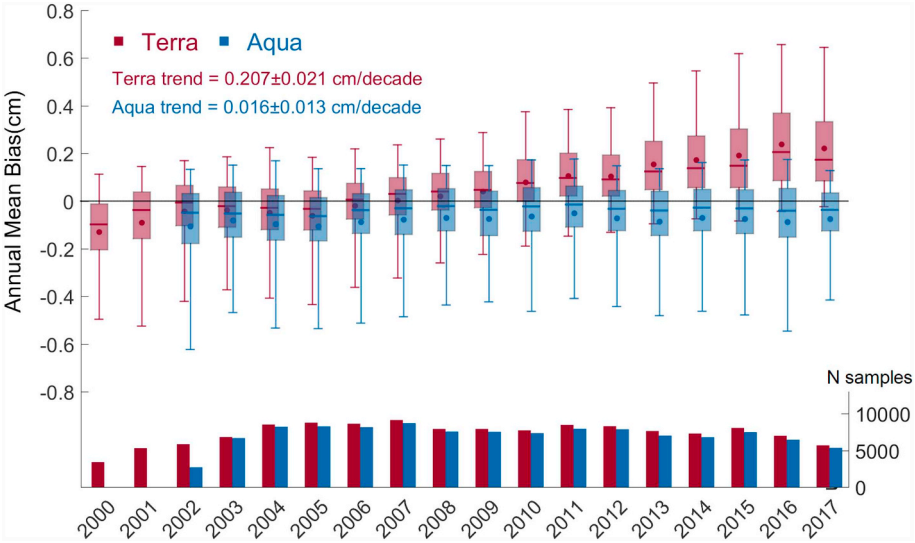


**Fig. 10.** Time series of annual mean bias of CWV derived from MAIAC (MCD19A2) versus AERONET records. The y-axis values represent the difference of MAIAC – AERONET CWV. The number of annual samples is presented in the bottom. Both calculated trends are significantly different from zero at a 95% confidence level.

then, it increases for most regions during 2008–2017 period. These findings imply that these products are diverging from each other and leading to artificial trends in the CWV magnitude over time. Note that this discrepancy is also seasonally dependent (e.g. East North America), with larger offsets occurring in the wet season.

The sensor degradation and calibration drift could introduce a systematic offset in the data products. In this context, further evaluation is performed using long-term AERONET sites (79) with > 15 years of collocated data. Fig. 10 shows annual mean biases (y-axis) versus time (x-axis) for both sensor products. We found a systematic upward trend in $MAIAC_T$ retrievals, with decadal change of 0.207 ± 0.021 cm ($p < .05$). The annual mean bias of $MAIAC_T$ is negative between 2000 and 2006, and then, it shifts to positive biases from 2007 to 2017. In contrast, $MAIAC_A$ retrievals are more stable over time, with a small change (0.016 cm/decade, $p$-value < .05). Thus, any temporal analysis should account for the mentioned calibration trends.

## 4. Discussion

This study presents a global validation of CWV product from MODIS C6 MAIAC (MCD19A2). This product was globally evaluated using 265 AERONET sites within 2000–2017 period. While some studies have evaluated the MAIAC aerosol product (Superczynski et al., 2017; Martins et al., 2017a; Lyapustin et al., 2018; Mhawish et al., 2019), this study is the first validation of operational MAIAC CWV (MCD19A2) product at global-scale. The overall comparison is shown in the Fig. 3 and Table 1 revealing a good agreement between MAIAC/AERONET observations (R ~ 0.975 and RMSE < 0.250 cm). Overall, this performance is similar or better than other satellite-derived CWV products (Li et al., 2003; Raja et al., 2008; Schrijver et al., 2009; Mears et al., 2015; Wang et al., 2016; Bright et al., 2018). For instance, Diedrich et al. (2015) show that the standard MODIS water vapor (MOD05) overestimates retrievals by about ~20% compared to globally AERONET observations (2003–2014), with RMSE of 0.335 cm. Lindstrot et al. (2012) found an RMSE of 0.29 cm for MERIS (Medium Resolution Imaging Spectrometer) CWV retrievals against AERONET data (2003–2005). These examples illustrate that MAIAC CWV is also consistent with well-established products, and the overall comparison has proven the quality of CWV retrievals.

The results show that MAIAC accuracy varies according to the water vapor magnitude and sensor product (Figs. 5 and 6). We observed an underestimation of $MAIAC_A$ retrievals at high-CWV retrievals (dry bias), while $MAIAC_T$ retrievals show a near-zero mean bias. The local analysis shows similar difference between Terra (small positive bias) and Aqua (negative bias) CWV for most sites (Fig. 6). These findings highlight the challenges for coupling Terra and Aqua water vapor products (e.g. Martins et al., 2017b, 2018b). In addition, this study confirms that the expected error of MAIAC water vapor is about ± 15% (Table 1), with > 68% retrievals falling within EE envelope. This overall accuracy is within the range of standard MODIS L2 product (Gao and Kaufman, 2003). We observed that MAIAC performance is also regionally dependent (Table 2) and some regions may have a lower error (5–10%), such as South America, Middle East, and Europe for Aqua retrievals. Similarly, several studies have demonstrated a distinct accuracy of MOD05 product between regions, such as India (Prasad and Singh, 2009), Europe (Gui et al., 2017), China (Shi et al., 2018). In general, this variability is driven by the land surface properties, presence of haze (heavy aerosol), instrument calibration and water vapor regimes between regions (Kaufman and Gao, 1992; Gao and Kaufman, 2003; Diedrich et al., 2015). Particularly, the spectral change of surface reflectance in the 0.94 μm region could lead to substantial error on estimated transmittance, and consequently, on the water vapor retrieval. Lyapustin and Wang (2008) evaluated different approaches for MODIS water vapor retrievals, and they found a lower noise (2–3 factor) in the three-band approach in the narrow interval (0.9–0.94 μm) compared to five-band approach from Gao and Kaufman (2003). Indeed, the regional performance is satisfactory (Table 2) and confirms the ability of MAIAC algorithm to provide reliable dataset across several conditions.

The EOS MODIS instruments have successfully operated for almost two decades, but they have far exceeded their design lifetime (6-year). The MODIS Characterization Support Team (https://mcst.gsfc.nasa.gov/) has made an extensive effort to maintain well-calibrated data over its entire mission (Sun et al., 2012; Toller et al., 2013). However, due to the long life of these instruments, careful analysis of temporal offset is relevant to assure the consistency of MAIAC MCD19A2 product. The global average of CWV shows a systematic offset (~0.3–0.5 cm) between Terra and Aqua products (Fig. 9). The larger discrepancies were observed for humid areas such as Amazon rainforest (up to 1.0 cm) compared to those in the Sahara Desert (up to 0.4 cm). The results shown in Fig. 10 revealed a gradual error change of $MAIAC_T$ compared to AERONET observations. The decadal change of $MAIAC_T$ is about +0.207 cm, shifting from negative (pre-2006) to positive bias values in recent years. In contrast, $MAIAC_A$ retrievals are temporally

stable with a small trend (~0.02 cm/decade). Undeniably, these time-dependent biases are critical for long-term studies focused on climate signals, because it could lead to misinterpretation of the temporal variability, especially in humid regions. While this study did not specifically investigate the calibration trends, the impacts of sensor degradation and calibration drift are evident in this analysis, especially for MODIS Terra. In fact, recent studies have evaluated the Terra/Aqua consistency for aerosol retrievals over time (Levy et al., 2010; Sayer et al., 2015; Levy et al., 2018). Particularly, Levy et al. (2010) found a significant trend in Collection 5 Terra AOD retrievals, with an apparent offset of Aqua retrievals over land. The MODIS Collection 6 reprocessing over land has corrected most calibration trends (e.g. Lyapustin et al. (2014b)), however, that analysis did not involve the MODIS NIR channels (B17–19) used in the water vapor algorithm. This study reveals that further calibration analysis is needed for MODIS B17–19.

## 5. Summary and conclusions

In this paper, we present a global validation of water vapor derived from MODIS C6 MAIAC (MCD19A2) over land. This validation gives a detailed picture of the global and regional performance of MAIAC CWV using 265 AERONET locations for 2000–2017. We summarize our findings as follows:

i) Global performance: The new operational MAIAC (MCD19A2) product derives reliable CWV retrievals for both MODIS Terra and Aqua products. A strong correlation was found between MAIAC/AERONET observations ($R > 0.95$ and RMSE < 0.25 cm) (Fig. 3). The expected error of this product was defined as ± 15%, with > 68% of retrievals falling within this envelope. We found underestimation of CWV from Aqua in humid conditions (dry bias), while the Terra retrievals are more stable (Fig. 5).

ii) Local and regional variability: The statistics are satisfactory for all regions, but MAIAC performance is regionally dependent and varies between two sensors. For instance, the regions such as South America, Oceania and Europe present remarkable performance in terms of EE values for Aqua. In the local analysis, we found a different mean bias for Terra (positive) and Aqua (negative) products in most sites. The RMSE increases with atmospheric moisture and is typically higher in the tropics compared to the temperate regions.

iii) Time series analysis: A systematic offset (~0.3–0.5 cm) between Terra and Aqua retrievals was found over the period of 2000–2017. This discrepancy is larger in the tropical humid region (e.g. Amazon) compared to the dry areas (e.g. Sahara Desert). The temporal offset (Terra-Aqua) is stable during 2002–2007, and then, it increases from 2008 to 2017. We also observed a gradual change of MAIAC CWV bias over time, mostly in MODIS Terra. These findings are relevant for the scientific community using MODIS C6 CWV products. The MODIS science team is working on the residual trend correction to implement in the Collection 6.1 reprocessing.

Finally, this validation shows that MCD19A2 (C6) CWV provides a reliable dataset for both sensor products over land, and the scientific community can explore a wide variety of applications using this new operational product.

## Acknowledgements

We thank NASA MODIS team for providing the Level-2 MCD19A2 data products (https://ladsweb.modaps.eosdis.nasa.gov/). We also thank the AERONET project at NASA/GSFC for providing the ground-based aerosol data (https://aeronet.gsfc.nasa.gov/). We would like to thank the principal investigators and their staff for maintaining instrumentation and processing these data. We are grateful to the Dr. Brent Holben (AERONET PI) for supporting this study. We thank the anonymous reviewers for their comments.

## References

Alexandrov, M.D., Schmid, B., Turner, D.D., Cairns, B., Oinas, V., Lacis, A.A., ... Eilers, J., 2009. Columnar water vapor retrievals from multifilter rotating shadow band radiometer data. J. Geophys. Res. 114 (D2).

Allan, R.P., Soden, B.J., 2008. Atmospheric warming and the amplification of precipitation extremes. Science 321 (5895), 1481–1484.

Bennouna, Y.S., Torres, B., Cachorro, V.E., Ortiz de Galisteo, J.P., Toledano, C., 2013. The evaluation of the integrated water vapour annual cycle over the Iberian Peninsula from EOS-MODIS against different ground-based techniques. Q. J. R. Meteorol. Soc. 139 (676), 1935–1956.

Bevis, M., Businger, S., Herring, T.A., Rocken, C., Anthes, R.A., Ware, R.H., 1992. GPS meteorology: Remote sensing of atmospheric water vapor using the Global Positioning System. J. Geophys. Res. 97 (D14), 15787–15801.

Bokoye, A.I., Royer, A., Cliche, P., O'Neill, N., 2007. Calibration of sun radiometer–based atmospheric water vapor retrievals using GPS meteorology. J. Atmos. Ocean. Technol. 24 (6), 964–979.

Bright, J.M., Gueymard, C.A., Killinger, S., Lingfors, D., Sun, X., Wang, P., Engerer, N.A., 2018. Climatic and global validation of daily MODIS precipitable water data at AERONET sites for clear-sky irradiance modelling. In: EuroSun, pp. 2018.

Chu, D.A., Kaufman, Y.J., Ichoku, C., Remer, L.A., Tanré, D., Holben, B.N., 2002. Validation of MODIS aerosol optical depth retrieval over land. Geophys. Res. Lett. 29 (12) (MOD2-1).

Colman, R., 2003. A comparison of climate feedbacks in general circulation models. Clim. Dyn. 20 (7–8), 865–873.

Dessler, A.E., Wong, S., 2009. Estimates of the water vapor climate feedback during El Niño–Southern Oscillation. J. Clim. 22 (23), 6404–6412.

Dessler, A.E., Zhang, Z., Yang, P., 2008. Water-vapor climate feedback inferred from climate fluctuations, 2003–2008. Geophys. Res. Lett. 35 (20).

Diedrich, H., Preusker, R., Lindstrot, R., Fischer, J., 2015. Retrieval of daytime total columnar water vapour from MODIS measurements over land surfaces. Atmos. Meas. Tech. 8 (2), 823–836.

Dubovik, O., Holben, B., Eck, T.F., Smirnov, A., Kaufman, Y.J., King, M.D., Slutsker, I., 2002. Variability of absorption and optical properties of key aerosol types observed in worldwide locations. J. Atmos. Sci. 59 (3), 590–608.

Durre, I., Vose, R.S., Wuertz, D.B., 2006. Overview of the integrated global radiosonde archive. J. Clim. 19 (1), 53–68.

Fragkos, K., Antonescu, B., Ene, D., Efstathiou, G.A., Belegante, L., 2018. Assessment of the total precipitable water from a sun-photometer, microwave radiometer and radiosondes at a continental site in southeastern Europe. Atmos. Meas. Tech. Discuss. https://doi.org/10.5194/amt-2018-237. (in review).

Frouin, R., Deschamps, P.Y., Lecomte, P., 1990. Determination from space of atmospheric total water vapor amounts by differential absorption near 940 nm: theory and airborne verification. J. Appl. Meteorol. 29 (6), 448–460.

Gao, B.C., Kaufman, Y.J., 2003. Water vapor retrievals using Moderate Resolution Imaging Spectroradiometer (MODIS) near-infrared channels. J. Geophys. Res. Atmos. 108 (D13).

Giles, D.M., Sinyuk, A., Sorokin, M.G., Schafer, J.S., Smirnov, A., Slutsker, I., ... Welton, E.J., 2019. Advancements in the Aerosol Robotic Network (AERONET) Version 3 database–automated near-real-time quality control algorithm with improved cloud screening for Sun photometer aerosol optical depth (AOD) measurements. Atmos. Meas. Tech. 12 (1), 169–209.

Gui, K., Che, H., Chen, Q., Zeng, Z., Liu, H., Wang, Y., ... Zhang, X., 2017. Evaluation of radiosonde, MODIS-NIR-Clear, and AERONET precipitable water vapor using IGS ground-based GPS measurements over China. Atmos. Res. 197, 461–473.

Halthore, R.N., Eck, T.F., Holben, B.N., Markham, B.L., 1997. Sun photometric measurements of atmospheric water vapor column abundance in the 940-nm band. J. Geophys. Res. 102 (D4), 4343–4352.

Held, I.M., Soden, B.J., 2000. Water vapor feedback and global warming. Annu. Rev. Energy Environ. 25 (1), 441–475.

Hilker, T., Lyapustin, A.I., Tucker, C.J., Sellers, P.J., Hall, F.G., Wang, Y., 2012. Remote sensing of tropical ecosystems: Atmospheric correction and cloud masking matter. Remote Sens. Environ. 127, 370–384.

Holben, B.N., Eck, T.F., Slutsker, I., Tanre, D., Buis, J.P., Setzer, A., ... Lavenu, F., 1998. AERONET—a federated instrument network and data archive for aerosol characterization. Remote Sens. Environ. 66 (1), 1–16.

IPCC, 2007. The Physical Science Basis. In: Contribution of Working Group I to the Fourth Assessment Report of the *International Panel on Climate Change*. vol. *4*. Cambridge University Press, pp. 2007.

Justice, C.O., Vermote, E., Townshend, J.R., Defries, R., Roy, D.P., Hall, D.K., ... Lucht, W., 1998. The moderate resolution imaging Spectroradiometer (MODIS): land remote sensing for global change research. IEEE Trans. Geosci. Remote Sens. 36 (4), 1228–1249.

Kaufman, Y.J., Gao, B.C., 1992. Remote sensing of water vapor in the near IR from EOS/MODIS. IEEE Trans. Geosci. Remote Sens. 30 (5), 871–884.

King, M.D., Kaufman, Y.J., Menzel, W.P., Tanre, D., 1992. Remote sensing of cloud, aerosol, and water vapor properties from the Moderate Resolution Imaging Spectrometer(MODIS). IEEE Trans. Geosci. Remote Sens. 30 (1), 2–27.

Levy, R.C., Remer, L.A., Kleidman, R.G., Mattoo, S., Ichoku, C., Kahn, R., Eck, T.F., 2010. Global evaluation of the Collection 5 MODIS dark-target aerosol products over land. Atmos. Chem. Phys. 10 (21), 10399–10420.

Levy, R.C., Mattoo, S., Sawyer, V., Shi, Y., Colarco, P.R., Lyapustin, A.I., ... Remer, L.A., 2018. Exploring systematic offsets between aerosol products from the two MODIS sensors. Atmos. Meas. Tech. 11 (7), 4073–4092.

Li, Z., Muller, J.P., Cross, P., 2003. Comparison of precipitable water vapor derived from

radiosonde, GPS, and Moderate-Resolution Imaging Spectroradiometer measurements. J. Geophys. Res. 108 (D20).
Lindstrot, R., Preusker, R., Diedrich, H., Doppler, L., Bennartz, R., Fischer, J., 2012. 1D-Var retrieval of daytime total columnar water vapour from MERIS measurements. Atmos. Meas. Tech. 5 (3), 631–646.
Lyapustin, A.I., 2003. Interpolation and Profile Correction (IPC) method for shortwave radiative transfer in spectral intervals of gaseous absorption. J. Atmos. Sci. 60 (6), 865–871.
Lyapustin, A., Wang, Y., 2008. MAIAC–Multi-angle implementation of atmospheric correction for MODIS. In: Algorithm Theoretical Basis Document.
Lyapustin, A., Wang, Y., Frey, R., 2008. An automatic cloud mask algorithm based on time series of MODIS measurements. J. Geophys. Res. 113 (D16).
Lyapustin, A., Wang, Y., Laszlo, I., Kahn, R., Korkin, S., Remer, L., Levy, R., Reid, J.S., 2011. Multiangle implementation of atmospheric correction (MAIAC): 2. Aerosol algorithm. J. Geophys. Res. 116 (D3).
Lyapustin, A.I., Wang, Y., Laszlo, I., Hilker, T., Hall, F.G., Sellers, P.J., ... Korkin, S.V., 2012. Multi-angle implementation of atmospheric correction for MODIS (MAIAC): 3. Atmospheric correction. Remote Sens. Environ. 127, 385–393.
Lyapustin, A., Alexander, M.J., Ott, L., Molod, A., Holben, B., Susskind, J., Wang, Y., 2014a. Observation of mountain lee waves with MODIS NIR column water vapor. Geophys. Res. Lett. 41 (2), 710–716.
Lyapustin, A., Wang, Y., Xiong, X., Meister, G., Platnick, S., Levy, R., ... Hall, F., 2014b. Scientific impact of MODIS C5 calibration degradation and C6+ improvements. Atmos. Meas. Tech. 7 (12), 4353–4365.
Lyapustin, A., Wang, Y., Korkin, S., Huang, D., 2018. MODIS collection 6 MAIAC algorithm. Atmos. Meas. Tech. Discuss. 1–50.
Martins, V.S., Lyapustin, A., de Carvalho, L.A.S., Barbosa, C.C.F., Novo, E.M.L.M., 2017a. Validation of high-resolution MAIAC aerosol product over South America. J. Geophys. Res. 122 (14), 7537–7559.
Martins, V., Barbosa, C., de Carvalho, L., Jorge, D., Lobo, F., Novo, E., 2017b. Assessment of atmospheric correction methods for Sentinel-2 MSI images applied to Amazon floodplain lakes. Remote Sens. 9 (4), 322.
Martins, V.S., Novo, E.M., Lyapustin, A., Aragão, L.E., Freitas, S.R., Barbosa, C.C., 2018a. Seasonal and interannual assessment of cloud cover and atmospheric constituents across the Amazon (2000–2015): Insights for remote sensing and climate analysis. ISPRS J. Photogramm. Remote Sens. 145, 309–327.
Martins, V.S., Soares, J.V., Novo, E.M., Barbosa, C.C., Pinto, C.T., Arcanjo, J.S., Kaleita, A., 2018b. Continental-scale surface reflectance product from CBERS-4 MUX data: assessment of atmospheric correction method using coincident Landsat observations. Remote Sens. Environ. 218, 55–68.
Mears, C.A., Wang, J., Smith, D., Wentz, F.J., 2015. Intercomparison of total precipitable water measurements made by satellite-borne microwave radiometers and ground-based GPS instruments. J. Geophys. Res. 120 (6), 2492–2504.
Mhawish, A., Banerjee, T., Sorek-Hamer, M., Lyapustin, A., Broday, D.M., Chatfield, R., 2019. Comparison and evaluation of MODIS Multi-angle Implementation of Atmospheric Correction (MAIAC) aerosol product over South Asia. Remote Sens. Environ. 224, 12–28.
Michalsky, J.J., Min, Q., Kiedron, P.W., Slater, D.W., Barnard, J.C., 2001. A differential technique to retrieve column water vapor using sun radiometry. J. Geophys. Res. 106 (D15), 17433–17442.
Ortiz de Galisteo, J.P., Bennouna, Y., Toledano, C., Cachorro, V., Romero, P., Andrés, M.I., Torres, B., 2014. Analysis of the annual cycle of the precipitable water vapour over Spain from 10-year homogenized series of GPS data. Q. J. R. Meteorol. Soc. 140 (679), 397–406.
Parkinson, C.L., 2013. Summarizing the first ten years of NASA's Aqua mission. IEEE J. Sel. Top. Appl. Earth Obs. Remote. Sens. 6 (3), 1179–1188.
Pérez-Ramírez, D., Whiteman, D.N., Smirnov, A., Lyamani, H., Holben, B.N., Pinker, R., ... Alados-Arboledas, L., 2014. Evaluation of AERONET precipitable water vapor versus microwave radiometry, GPS, and radiosondes at ARM sites. J. Geophys. Res. 119 (15), 9596–9613.
Prasad, A.K., Singh, R.P., 2009. Validation of MODIS Terra, AIRS, NCEP/DOE AMIP-II Reanalysis-2, and AERONET Sun photometer derived integrated precipitable water vapor using ground-based GPS receivers over India. J. Geophys. Res. 114 (D5).
Raja, M.R.V., Gutman, S.I., Yoe, J.G., McMillin, L.M., Zhao, J., 2008. The validation of AIRS retrievals of integrated precipitable water vapor using measurements from a network of ground-based GPS receivers over the contiguous United States. J. Atmos. Ocean. Technol. 25 (3), 416–428.
Reagan, J., Thome, K., Herman, B., Stone, R., Deluisi, J., Snider, J., 1995. A comparison of columnar water vapor retrievals obtained with near-IR solar radiometer and microwave radiometer measurements. J. Appl. Meteorol. 34 (6), 1384–1391.
Remer, L.A., Kaufman, Y.J., Tanré, D., Mattoo, S., Chu, D.A., Martins, J.V., ... Eck, T.F., 2005. The MODIS aerosol algorithm, products, and validation. J. Atmos. Sci. 62 (4), 947–973.
Rind, D., Chiou, E.W., Chu, W., Larsen, J., Oltmans, S., Lerner, J., ... McMaster, L., 1991. Positive water vapour feedback in climate models confirmed by satellite data. Nature 349 (6309), 500.
Rocken, C., Ware, R., Van Hove, T., Solheim, F., Alber, C., Johnson, J., ... Businger, S., 1993. Sensing atmospheric water vapor with the Global Positioning System. Geophys. Res. Lett. 20 (23), 2631–2634.
Sayer, A.M., Hsu, N.C., Bettenhausen, C., Jeong, M.J., Meister, G., 2015. Effect of MODIS Terra radiometric calibration improvements on Collection 6 Deep Blue aerosol products: Validation and Terra/Aqua consistency. J. Geophys. Res. 120 (23), 12–157.
Schläpfer, D., Borel, C.C., Keller, J., Itten, K.I., 1998. Atmospheric precorrected differential absorption technique to retrieve columnar water vapor. Remote Sens. Environ. 65 (3), 353–366.
Schmid, B., Thorne, K.J., Demoulin, P., Peter, R., Mätzler, C., Sekler, J., 1996. Comparison of modeled and empirical approaches for retrieving columnar water vapor from solar transmittance measurements in the 0.94-μm region. J. Geophys. Res. 101 (D5), 9345–9358.
Schmid, B., Michalsky, J.J., Slater, D.W., Barnard, J.C., Halthore, R.N., Liljegren, J.C., Ingold, T., 2001. Comparison of columnar water-vapor measurements from solar transmittance methods. Appl. Opt. 40 (12), 1886–1896.
Schrijver, H., Gloudemans, A.M.S., Frankenberg, C., Aben, I., 2009. Water vapour total columns from SCIAMACHY spectra in the 2.36 μm window. Atmos. Meas. Tech. 2 (2), 561–571.
Seidel, D.J., Randel, W.J., 2006. Variability and trends in the global tropopause estimated from radiosonde data. J. Geophys. Res. 111 (D21).
Sherwood, S.C., Roca, R., Weckwerth, T.M., Andronova, N.G., 2010. Tropospheric water vapor, convection, and climate. Rev. Geophys. 48 (2).
Shi, F., Xin, J., Yang, L., Cong, Z., Liu, R., Ma, Y., ... Zhao, L., 2018. The first validation of the precipitable water vapor of multisensor satellites over the typical regions in China. Remote Sens. Environ. 206, 107–122.
Smirnov, A., Holben, B.N., Lyapustin, A., Slutsker, I., Eck, T.F., 2004. AERONET Processing Algorithms Refinement, Paper Presented at AERONET Workshop (El Arenosillo, Spain). pp. 10–14 (May).
Soden, B.J., 2000. Atmospheric physics: enlightening water vapour. Nature 406 (6793), 247.
Sun, J., Angal, A., Xiong, X., Chen, H., Geng, X., Wu, A., ... Chu, M., 2012. MODIS reflective solar bands calibration improvements in Collection 6. In: Earth Observing Missions and Sensors: Development, Implementation, and Characterization II. vol. 8528. International Society for Optics and Photonics, pp. 85280N November.
Superczynski, S.D., Kondragunta, S., Lyapustin, A.I., 2017. Evaluation of the multi-angle implementation of atmospheric correction (MAIAC) aerosol algorithm through intercomparison with VIIRS aerosol products and AERONET. J. Geophys. Res. 122 (5), 3005–3022.
Toller, G., Xiong, X.J., Sun, J., Wenny, B.N., Geng, X., Kuyper, J., ... Wu, A., 2013. Terra and Aqua moderate-resolution imaging spectroradiometer collection 6 level 1B algorithm. J. Appl. Remote. Sens. 7 (1), 073557.
Torres, B., Cachorro, V.E., Toledano, C., Ortiz de Galisteo, J.P., Berjón, A., De Frutos, A.M., ... Laulainen, N., 2010. Precipitable water vapor characterization in the Gulf of Cadiz region (southwestern Spain) based on Sun photometer, GPS, and radiosonde data. J. Geophys. Res. 115 (D18).
Trenberth, K.E., Fasullo, J., Smith, L., 2005. Trends and variability in column-integrated atmospheric water vapor. Clim. Dyn. 24 (7–8), 741–758.
Vaquero-Martínez, J., Antón, M., de Galisteo, J.P.O., Cachorro, V.E., Costa, M.J., Román, R., Bennouna, Y.S., 2017. Validation of MODIS integrated water vapor product against reference GPS data at the Iberian Peninsula. Int. J. Appl. Earth Obs. Geoinf. 63, 214–221.
Vaquero-Martínez, J., Antón, M., de Galisteo, J.P.O., Cachorro, V.E., Álvarez-Zapatero, P., Román, R., ... Noël, S., 2018. Inter-comparison of integrated water vapor from satellite instruments using reference GPS data at the Iberian Peninsula. Remote Sens. Environ. 204, 729–740.
Wang, H., Abad, G.G., Liu, X., Chance, K., 2016. Validation and update of OMI Total ColumnWater Vapor product. Atmos. Chem. Phys. 16 (17).